The Thesis Committee for Andrea Haessly Dickson
Certifies that this is the approved version of the following thesis:

Investigation of firing properties in CA1 hippocampal pyramidal neurons in a mouse model of Fragile X syndrome

APPROVED BY
SUPERVISING COMMITTEE:

Supervisor:

Daniel Johnston

Richard Aldrich

Investigation of firing properties of CA1 hippocampal pyramidal neurons in a mouse model of Fragile X syndrome

by

Andrea Haessly Dickson, B.S.; M.S.C.S.

Thesis

Presented to the Faculty of the Graduate School of

The University of Texas at Austin

in Partial Fulfillment

of the Requirements

for the Degree of

Master of Science in Neuroscience

The University of Texas at Austin

December 2012

Dedication

To my dad.

Acknowledgements

I would like to thank Professor Kristen Harris for her mentorship and contagious enthusiasm. I was so thrilled to present my work from her lab as a poster at SFN. Thanks to Professor Rick Aldrich for one of the best classes I've ever taken. Also thanks to Professor Mike Mauk for a fun and interesting rotation.

Thanks to Professor Dan Johnston for giving me the opportunity to work and learn in his lab. Many thanks to all the members of his lab who trained me, answered my questions, gave me suggestions, and encouraged me these past few years – specifically Dr. Randy Chitwood, Dr. Kelly Dougherty, Dr. Darrin Brager, Dr. Rick Gray, Dr. Nik Dembrow, Sachin Vaidya, Ann Clemens, Dr. Brian Kalmbach, Dr. Chung Sub Kim, Dr. Yul Young Park, Dr. Payne Chang, Brandy Routh, Eedann McCord, and Vicky Moya. I would also like to give special thanks to Dr. Jenni Siegel and Dr. Brenda Houck for their help and encouragement.

Abstract

Investigation of firing properties of CA1 hippocampal pyramidal neurons in a mouse model of fragile X syndrome

Andrea Haessly Dickson, M.S.Neurosci.

The University of Texas at Austin, 2012

Supervisor: Daniel Johnston

Fragile X Syndrome is the most common form of heritable cognitive disability. It is caused by a genetic mutation that leads to a lack of protein from the FMR1 gene. This protein (FMRP) is used to regulate the translation of many other proteins, thereby leading to a wide range of effects. Because the origin of this disease is based on the lack of a single protein, an animal model with construct validity can be used to investigate the potential effects leading to the symptoms of the disease.

Many studies have investigated the synaptic plasticity differences of CA1 pyramidal neurons between a mouse model of fragile X syndrome (KO) and a wild type mouse (WT). This study investigates the differences in firing properties of a CA1 pyramidal neuron between the KO and WT. Specifically, contributions of two ion channels are investigated: the Ca^{2+} and voltage activated potassium channel (BK) and the potassium channel (M) inhibited by the muscarinic acetylcholine receptor.

This study finds some differences that warrant further investigation, including differences in spike timing, spike width and the initial rate of rise of an action

potential. However, several areas of investigation yield subtle or confounding results, which may indicate that the CA1 pyramidal neurons affected by the lack of FMRP may make up more than one population.

Table of Contents

List of Figures

Chapter 1: Introduction

In humans, cognitive impairments can be caused by several factors, both environmental and genetic. The most common genetic cause of these impairments is Fragile X syndrome (FXS). FXS patients also display other characteristics such as childhood seizures, hyperactivity, hypersensitivity to stimuli, delayed language development, and limited eye contact. It is also the leading genetic cause of autism. This disease is caused by a lack of the fragile X protein (FMRP). A mutation upstream of the gene (FMR1), consisting of an excessive number (>200) of CGG repeats, causes a hyper-methylation of the region and blocks translation (Bell et al., 1991).

FMRP has several biological functions. It is most known for binding to mRNA/ribosomal complexes and suppressing translation. In neurons, it has also been implicated in mRNA transport and in activity-dependent, local translation. Interestingly, FMRP is also known to regulate it's own translation. In the disease, the lack of FMRP protein can lead to an overabundance of protein, differentially localized mRNA, and the disruption of signaling pathways that relied on activity dependent regulation of FMRP and its associated mRNA.

Because the source mutation is known and affects only one gene, a transgenic mouse has been created that lacks a functional FMR1 gene (KO) (Anon, 1994). The mouse has been used in comparison with a wild type mouse (WT) to investigate morphological, physiological and behavioral consequences of a lack of FMRP, as well as in evaluating the ability of potential drug therapies to reverse some of the differences.

In both humans and the mouse model of the disease there are striking morphological differences in the spines of pyramidal neurons (Galvez and Greenough, 2005; Grossman et al., 2006). In addition, studies of synaptic plasticity in the mouse

model have shown an increase in group I mGluR dependent LTD in the KO (Huber, 2002; Bear et al., 2004). The focus of research is expanding to include investigations of ion channels regulating the intrinsic properties of neurons including $K_V4.2$ (Gross et al., 2011; Lee et al., 2011), HCN (Brager et al., 2012), $K_V3.1$ (Strumbos et al., 2010), and the sodium-activated potassium channel Slack (Brown et al., 2010).

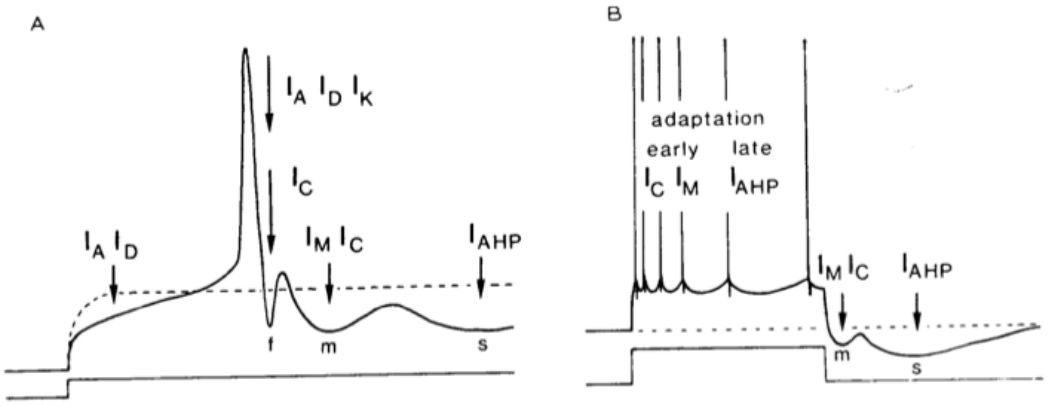

Figure 1.1: Various currents involved in the active properties of a neuron. A, currents that affect the wave form and after polarizations of an action potential. B, currents that affect the timing and after polarizations of multiple action potentials. Adapted from (Storm, 1990)

However, the output mechanism, via action potential firing, has not yet been investigated for this disease model. A binding study has shown that the mRNA of several ion channels involved in modulating the action potential waveform are possible targets of FMRP including: $Na_V1.2$, $Na_V1.6$, I_D channel $K_V1.2$, delayed rectifier $K_V2.1$, I_A channel $K_V4.2$, I_M channels $K_V7.2$ and $K_V7.3$, and the voltage and calcium activated potassium channel BK (Darnell et al., 2011). All of these channels can play a role in modulating the shape and timing of action potentials including threshold, width, height, and firing rate (Fig. 1.1) (Storm, 1990; Bean, 2007). I have investigated differences in action potential waveforms and in trains of action potentials between FMR1 knockout mice as compared

to wild type mice. I have pursued the involvement of BK channels and M-channels in these differences. I also have some proof of concept biochemical work needed to investigate the ion channels and structural proteins fomring the axon initial segment (AIS).

Chapter 2: General Methods

ANIMALS

Male mice with the background C57BL/6 from 2 to 3.5 months were used. Some mice carried a mutation where the FMR1 gene would not be expressed. The genotype of these animals is $FMR1^{-/y}$ and is referred to as FMR1 knockout (KO). The mice without the mutation are referred to as wild type (WT). Treatment of animals and experiments were within guidelines of the University of Texas at Austin IACUC.

SLICE PREPARATION

Mice were given a lethal injection of ketamine and xylazine. Once deeply anesthetized, mice were intracardially perfused with ice cold ACSF containing (in mM): 210 sucrose, 2.5 KCl, 1.2 NaH_2PO_4, 25 $NaHCO_3$, 0.5 CaCl2, 7.0 $MgCl_2$, and 7.0 dextrose bubbled with 95% O_2 / 5% CO_2. The brain was removed, bisected along the midline, and blocked for medial hippocampus. The brain was then mounted and 300 μm slices were obtained using a microtome. Slices were transferred to a holding chamber warmed to 35°C filled with ACSF containing (in mM): 125 NaCl, 2.5 KCl, 1.25 NaH_2PO_4, 25 $NaHCO_3$, 2 CaCl2, 2 $MgCl_2$, and 12.5 dextrose bubbled with 95% O_2 / 5% CO_2. Slices were maintained at 35°C for 30 minutes and then kept at room temperature until used.

ELECTROPHYSIOLOGY

Slices were transferred to a recording chamber perfused with 31-34°C ACSF similar to that in the holding chamber with the exception of 3 μM KCl. Borosilicate glass patch pipettes (3-6 MΩ) were filled with internal solution containing (in mM): 120 K-gluconate, 20 KCl, 11 HEPES, 4 NaCl, 4 MgATP, 0.3 Na-GTP, 7 K_2-phosphocreatine and 0.1 % neurobiotin adjusted to pH 7.3 unless otherwise noted.

Whole cell current clamp recordings were obtained using a Multiclamp 700B. Series resistance was continually monitored, and recordings where it exceeded 30 MΩ were discarded. Synaptic blockers were used in all experiments. Unless otherwise noted, the blocker concentrations used were (in μM): 20 DNQX, 50 AP5, and 2 gabazine.

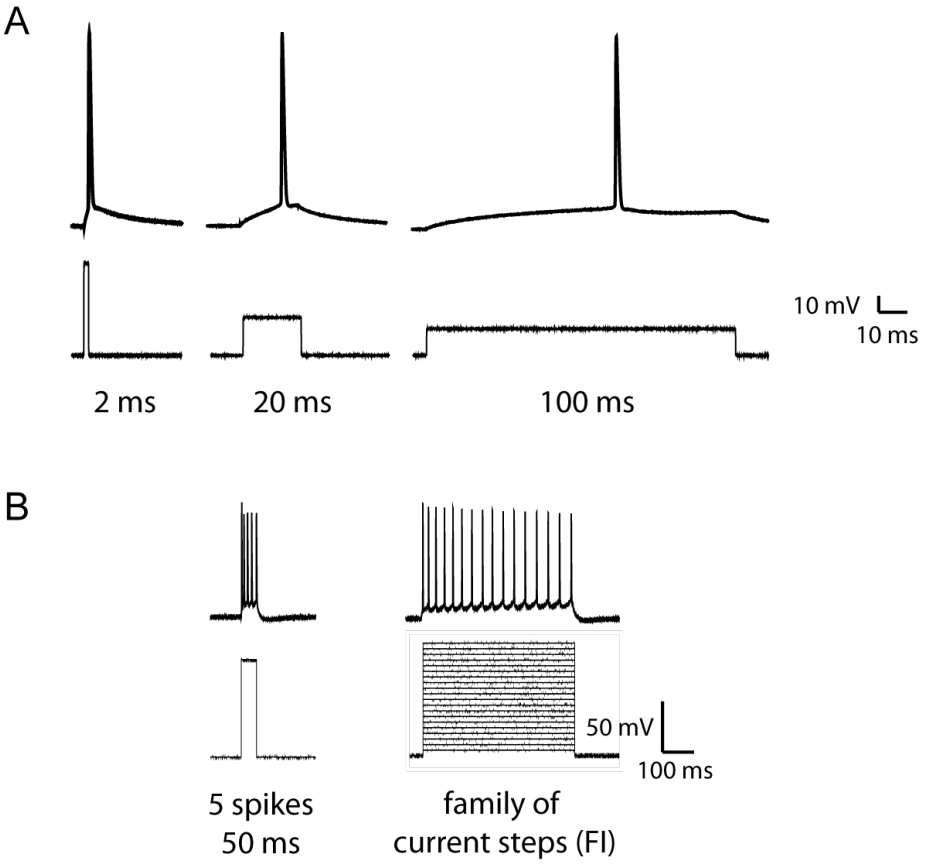

Figure 2.1: Spiking protocols. *A*, single spike protocols. *B*, action potential train protocols.

For most experiments, the membrane voltage (V_m) was adjusted to -65 mV by constant current injection. Input resistance (R_N) and rebound measurements were collected from a family of hyperpolarizing and depolarizing current steps. The maximum and steady state R_N were calculated as the slope of the current-voltage (IV) plots.

Maximum voltage values were measured as an average of 10 milliseconds (ms) around the peak of the voltage change (usually early in the trace). Steady state voltage values were measured as an average of a 50 ms window before the end of the step. The rebound slope is obtained from the steady state voltage plotted against the rebound amplitude from baseline.

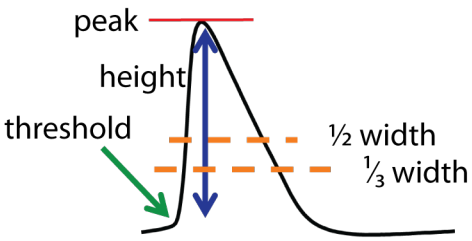

Figure 2.2: Measurements of single action potentials.

When taking measurements for single action potentials, three protocols that varied the length of the current injection were used: 2 ms, 20 ms, and 100 ms (Fig 2.1A). For each protocol, the amount of current injected was adjusted to elicit a single action potential timed to be close to the middle of the current injection. Threshold is measured as the point where the first derivative equals 20 mV/ms. Action potential height is measured from threshold to peak. Half width is the width of the action potential at ½ the height. Third width is the width of the action potential at 1/3 the height (Fig. 2.2). The maximum rate of change is the peak of the first derivative. The initial rate of change was the first derivative at two timepoints: 50 μs and 100 μs after threshold.

Two protocols were used to analyze trains of action potentials (Fig 2.1B). One protocol was a 50 ms current injection adjusted to yield 5 spikes (5sp). The final protocol was a family of depolarizing current injections 500 ms in length to invoke increasing numbers of action potentials (FI). Additional protocols will be specifically described in the chapters below.

DATA ACQUISITION AND ANALYSIS

In general recordings were sampled over 2x the filter rate. Recordings were digitized by an ITC-18 interface and captured by Axograph software. Wave analysis was performed by Axograph software.

STATISTICAL ANALYSIS

All data were expressed at mean ± SEM. Significance was determined by student's t-test when comparing 2 conditions. For more than 2 conditions a 2 factor ANOVA was used with Tukey's post hoc test. $p < 0.05$ was considered significant.

Chapter 3: Passive and active properties of CA1 pyramidal neurons in FMR1 knockout mice

INTRODUCTION

Passive properties of CA1 pyramidal cells were compared between FMR1 knockout mice and wild type mice to verify previous data reporting similarities in these properties at the soma (Brager et al., 2012). Several experiments were performed to determine what differences may exist in the firing properties of these cells between the WT and KO.

METHODS

Sampling and filtering rates used for these experiments were either 10 kHz sampling, 3 kHz filtering; or 50 kHz sampling, 10 kHz filtering.

RESULTS

There were no significant differences in the resting membrane potential, rebound or maximum and steady state input resistances between the WT and KO (Fig. 3.1). When comparing the properties of single spikes, no significant differences in threshold or spike peak were found (Fig 3.2. A, B). However, some significant differences were found related to the rate of rise of single spikes. The maximum of the first derivative of the 2 ms spike was significantly larger (i.e. faster) in the WT when compared to the KO (Fig. 3.2 C, $p=0.045$). The initial rate of rise, occurring 100 μs after threshold, was significantly larger in the WT for all three spiking protocols: 2 ms, 20 ms and 100 ms (Fig 3.2 D, $p=0.002$, $p=0.003$, $p=0.012$).

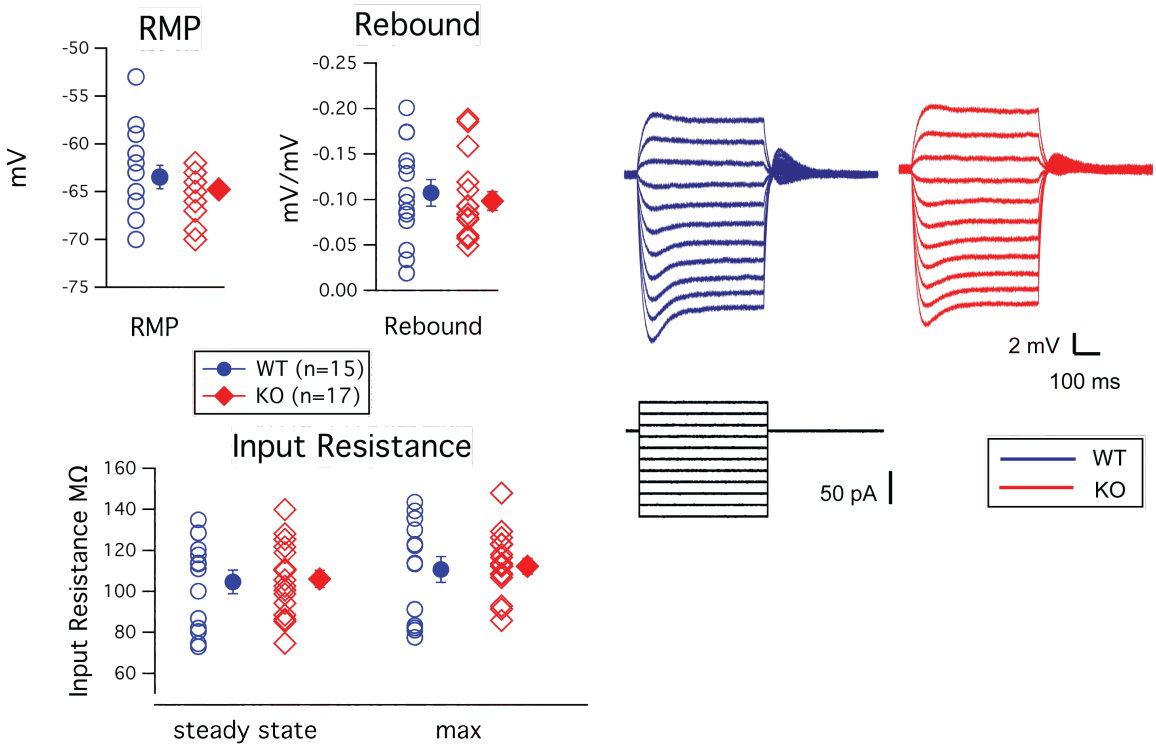

Figure 3.1: Comparison of passive properties between WT and KO.

Next, trains of action potentials were investigated. When comparing firing rate, the WT and KO were fairly similar; however, for smaller current injections the WT displayed a faster firing rate while for larger current injections the KO had a faster firing rate. This reached significance for current injections of 380 and 400 pA (Fig 3.3 p=0.044, 0.025). A subset of traces from the FI protocol where 16 spikes occurred was analyzed. The inter-spike interval (ISI) was calculated and the WT and KO values were compared. Early in the spike train, the KO had larger inter-spike intervals; but as the train continued, the WT showed more spike frequency adaptation resulting in ISIs that were smaller in the KO. The first, second and third intervals were significantly larger in the KO (Fig. 3.4 A

and B, p=0.006, 0.038 and 0.003). The last three intervals in the spike train were significantly smaller in the KO (Fig. 3.4 A and B, p=0.0001, 0.026 and 0.015).

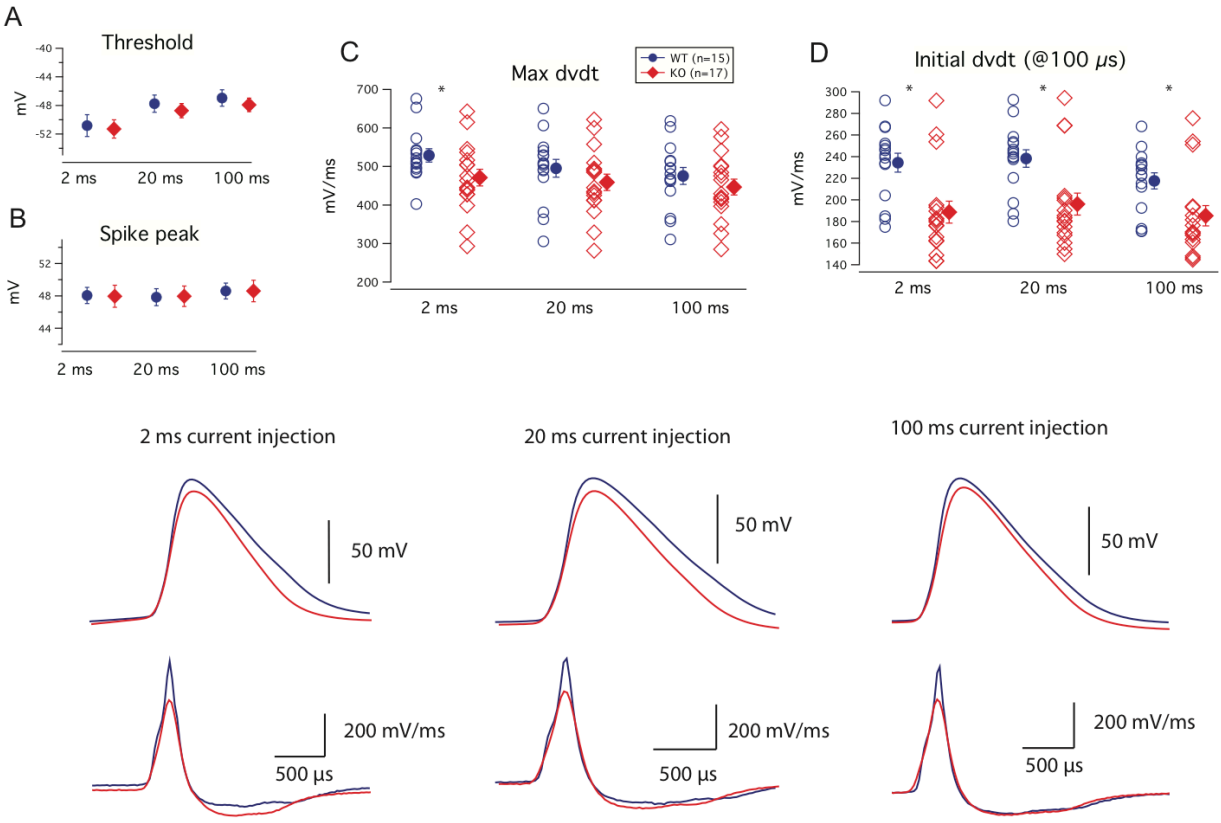

Figure 3.2: Comparison of spiking properties between WT and KO. * p<0.05.

The difference in spike amplitude between the first spike and last spike in the train were analyzed. The data is plotted based on the total number of spikes in the train (Fig. 3.5). As the number of spikes in a train increased (due to an increasing amount of current injected), the amplitude of the last spike was reduced more in the WT than in the

KO (7: p= 0.001, 10: p=0.044, 14: p=0.023, 16: p=0.029, 17: p=0.028, 18: p=0.031, 19: p=0.035, 20: p=0.005, 21: p=0.023, 22: p=0.009, 24: p=0.015, 25: p=0.015).

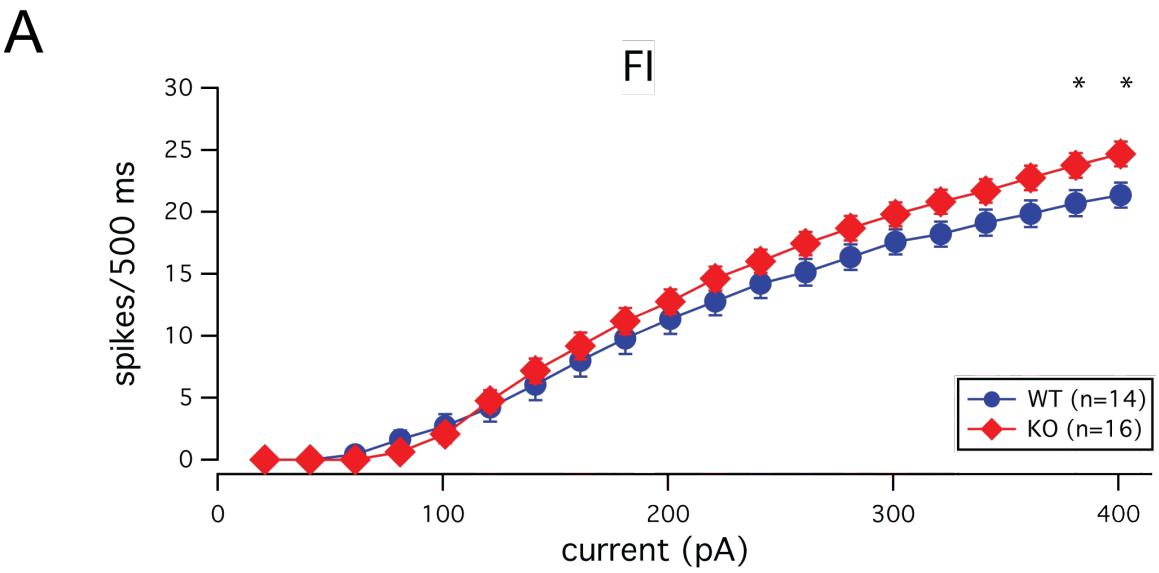

Figure 3.3: Firing rate plotted against current injection. * p<0.05.

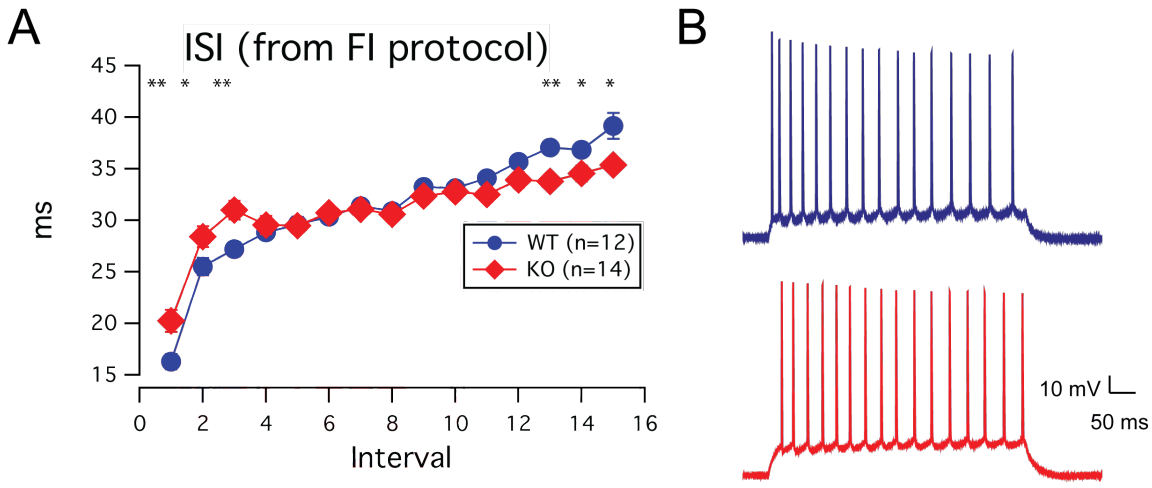

Figure 3.4: Comparison of spiking timing in a train containing 16 spikes. *A*, summary data for WT and KO. *B*, sample traces. ** p<0.01, * p<0.05.

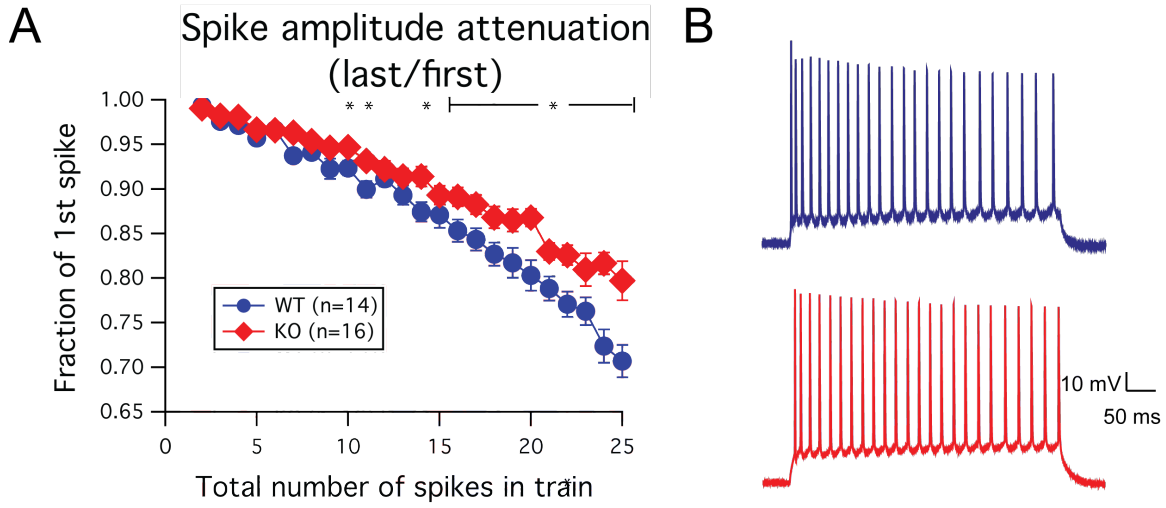

Figure 3.5: Comparison of spike amplitude attenuation in a train over an increasing number of spikes in a train. *A*, summary data for WT and KO. *B*, sample traces. ** p<0.01, * p<0.05.

DISCUSSION

The differences seen in the maximum slope of an action potential could be due to differences in various conductances. However, the fact that the differences are even more pronounced at very early time points of the action potential, 50 and 100 μs, indicates an involvement of the Na current. Somewhat surprising is that there was no significant difference in threshold even though there is a difference in initial slope.

Spike timing is influenced by several potassium conductances including the Ca^{2+} and voltage activated conductance BK, the small Ca^{2+} activated conductance SK, and a potassium conductance, M, which is activated at low voltages. Differences in BK and M currents are discussed in chapters 4 and 5 respectively.

The spike amplitude attenuation differences could be due to several possible conductances. These include inactivation of Na channels or activation of K channels such as the A-type channel.

Chapter 4: Contribution of BK channels in firing properties of CA1 pyramidal neurons in FMR1 knockout mice

INTRODUCTION

One of the significant differences found between wild type and FMR1 knockout mice is spike frequency adaptation, both early and late in a train. There are several ion channels that are known to have an effect on spike timing, two of which are Ca^{2+}-activated potassium channels (Lancaster and Adams, 1986; Lancaster and Nicoll, 1987; Gu et al., 2007). One of these channels is known as SK and has no voltage component to its activation. The other channel has a combined voltage and Ca^{2+} activation and is known as BK. SK has a relatively small conductance may contribute to the medium and slow hyperpolarizations after an action potential (AHP) for certain neuron types. BK has a large potassium conductance and is responsible for the fast AHP (Storm, 1987; Poolos and Johnston, 1999). Even though both of these channels are involved in spike timing, only mRNA of the alpha subunit of BK has been shown to be a candidate for regulation by FMRP (Darnell et al., 2011). Although there may be secondary effects of FMRP on SK, only BK was investigated.

Tetramers of the alpha subunit form the channel pore and contain the Ca^{2+} and voltage sensitive domains. There are 4 BK beta subunits (β1 – β4); however, only β2 and β4 are expressed in the brain. The β2 subunit confers inactivation and increases Ca^{2+} sensitivity. The β4 subunit modulates the Ca^{2+} sensitivity and causes the channel to be insensitive to block by iberiotoxin. On the other hand, BK channels are sensitive to block by paxilline regardless of associated subunit.

Paxilline was used during whole cell current clamp recordings to block BK channels. Data from WT and KO cells was compared both before and after application of

paxilline to investigate differential effects. Differential effects could indicate that FMRP is involved in the expression or function of the channel in CA1 pyramidal neurons.

METHODS

Electrophysiology

After experimental protocols are run initially, 10 μM paxilline, a BK channel blocker, is added to the external ACSF for the remainder of the experiment. Input resistance is monitored for 10 minutes to give the paxilline time to take effect. Then experimental protocols are executed a second time.

Sampling and filtering rates used for these experiments were either 10 kHz sampling, 3 kHz filtering; or 50 kHz sampling, 10 kHz filtering.

Statistical Analysis

To determine significant differences when comparing data including genotype and drug application, a two factor ANOVA was used. The drug application factor was treated as a repeated measure. Significant differences were determined using a post hoc Tukey's test.

RESULTS

For all three single spike protocols (2 ms, 20ms, and 100ms), 10 μM paxilline had the expected effect of increasing both the halfwidth and the width measured at 1/3 height (Fig 4.1). All spikes were significantly wider after paxilline application. Furthermore, the results indicated that the 1/3 width measurement was significantly different before application of paxilline for both the 2 ms protocol ($p=0.039$) and the 20 ms protocol ($p=0.019$). In both cases, the width of the action potentials is narrower in the KO.

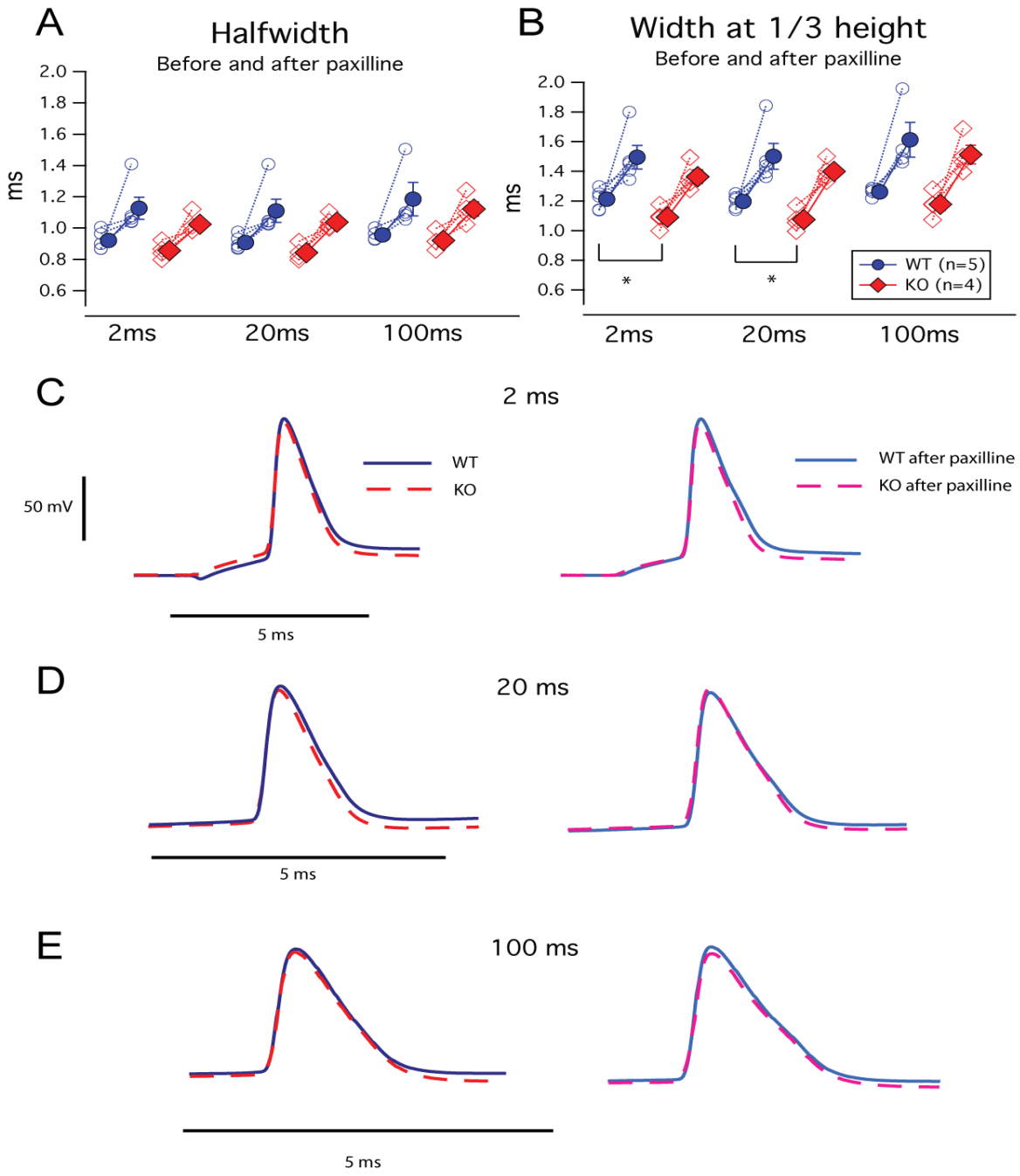

Figure 4.1: Comparison of width of single spikes between WT and KO both before and after application of BK channel blocker paxilline. *A*, summary data for the halfwidth measurement for the 2ms, 20 ms and 100 ms protocols. *B*, summary data for the 1/3 width measurement. The KO is significantly narrower for the 2 ms and the 20 ms protocols. *C, D, E*, representative traces for the 2 ms, 20 ms and 100 ms protocols respectively.

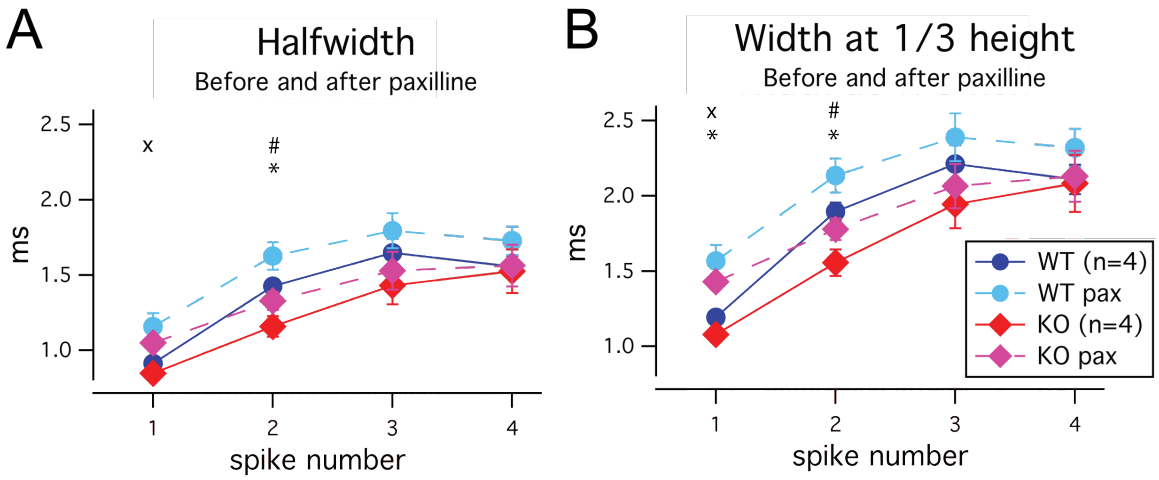

Figure 4.2: Comparison of width of spikes in a train between WT and KO both before and after paxilline application. *A*, halfwidth measurements for four spikes. *B*, 1/3 width measurements for four spikes. *: p<0.05 for WT vs. KO before paxilline application; #: p<0.05 for WT vs. KO after paxilline application; x: p <0.05 before vs. after paxilline application for genotype (applies to WT and KO separately).

Spike width was also analyzed for a train of spikes using the 5 spike protocol (Fig 4.2) although only the first 4 spikes were analyzed because the fifth spike could have occurred during the off step of the current injection. For the halfwidth measurement, the first spike was significantly different after paxilline application for both WT (p=0.038) and KO (p=0.002). Alternatively, the second spike was significantly different between the WT and KO mice both before (p=0.0194) and after paxilline application (p=0.033). Significant differences in the thirdwidth (Fig 4.2B) measurements were similar to that of halfwidth (first spike: WT p=0.013, KO p=0.001; second spike: before paxilline p=0.0188; after paxilline p=0.037) with the addition of a significant difference in the first spike between WT and KO before drug application (p=0.0366) (Fig 4.3A).

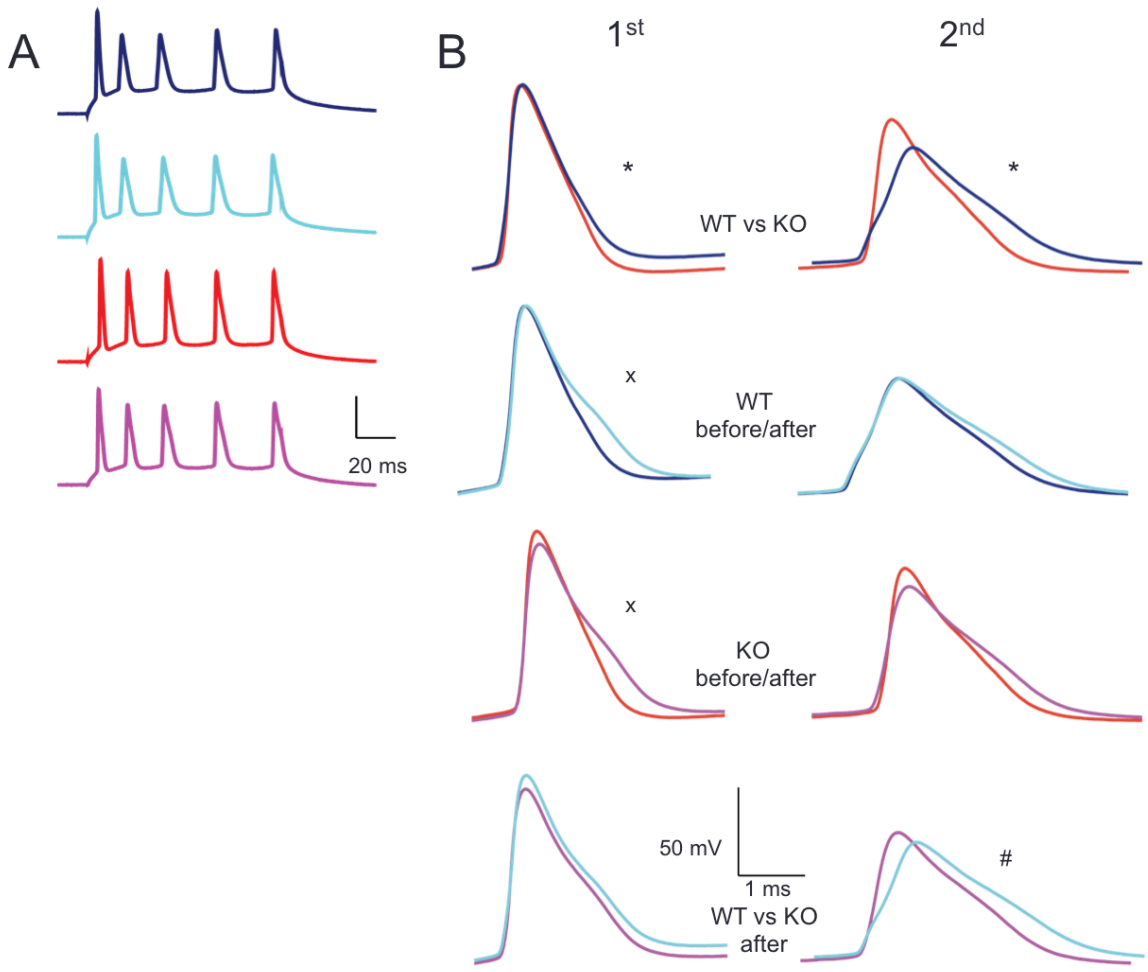

Figure 4.3: Traces from the 5 spike protocol. *A*. Representative traces from the 5 spike protocol for WT, WT after paxilline, KO and KO after paxilline. *B*. Overlays of the first spike and overlays of the second spike with significant differences in the width at 1/3 height indicated as in Fig 4.2B.

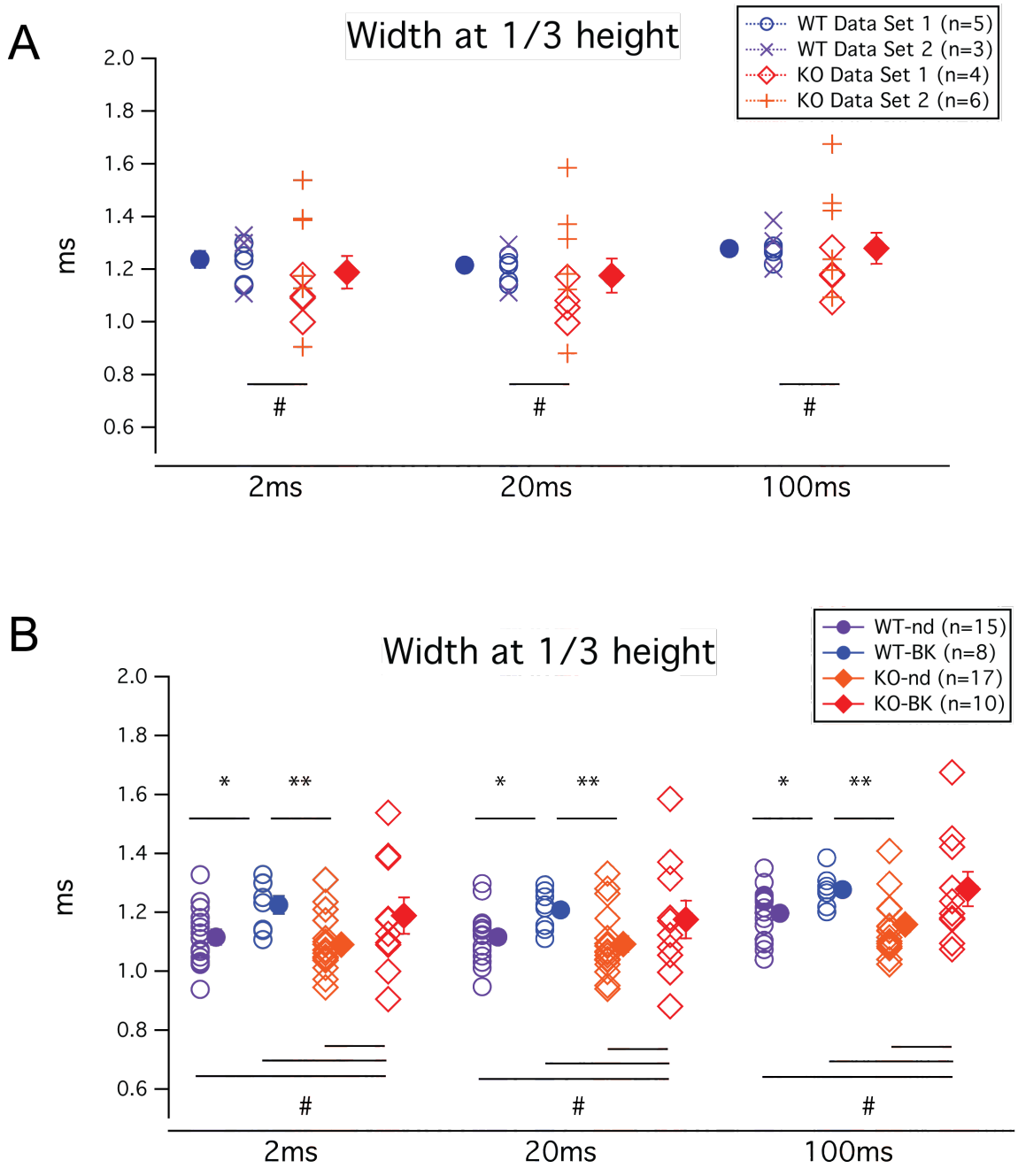

Figure 4.4: Larger datasets from WT and KO mice were compared with no drug. A, Data set 1 is from experiments where paxilline was subsequently applied. Data set 2 is from experiments where no post paxilline measurements were taken. B, data from experiments from Chapter 3 are compared with the merged data set from this chapter (labeled –BK). All significant differences in data sets (* $p < 0.05$, ** $p < 0.01$) and in variance (#) are shown.

Because significant differences were seen in the width measurements of single spikes before drug application, other data sets that had width measurements without drug application were added to the analysis. One of these data sets came from experiments where paxilline was applied but no post paxilline measurements were obtained (Fig 4.4A). With this expanded data set, no significant differences were found. However, the variance of the KO and WT data sets were different for each of the 3 protocols. Additionally, these combined data sets (WT-BK and KO-BK) were compared with data sets from experiments shown in Chapter 3 where no drug application was involved (WT-nd and KO-nd). The WT-BK measurements were significantly different from KO-nd measurements for all three protocols: 2 ms ($p=0.003$), 20 ms, ($p=0.004$) and 100 ms ($p=0.002$). Surprisingly, the WT-BK measurements were also significantly different from the WT-nd measurements for all three protocols (2 ms: $p=0.014$, 20 ms $p=0.012$, and 100 ms: $p=0.023$). Furthermore, when comparing the variance of these data sets, the KO-BK variance was different from each of the other three data sets, WT-BK, WT-nd, and KO-nd, for each of the three protocols. When the two WT data sets are merged and the two KO data sets are merged, the variances are different only for the 20 ms and 100 ms protocols.

DISCUSSION

The results from these paxilline experiments are not conclusive. Analysis of data before paxilline was applied shows significant differences in the width at 1/3 height of single action potentials elicited with a 2 ms or 20 ms current injection. However, when this data is combined with other experiments where post-paxilline measurements were not taken, no significant differences are seen. Instead more variability of the data is seen for the KO. This could indicate that there is more than one population of pyramidal cells

that have differing properties in the KO due to the lack of FMRP. Another possibility is that paxilline is not completely washed out of the chamber between experiments and residual paxilline has contaminated some of the data.

However, there are potential conclusions that can be drawn from the width of spikes in a train (Fig: 4.2). Only the first spike has a different width before and after paxilline application for both the WT and KO (Fig 4.3A). This indicates that BK has its greatest effect on these spikes. It is possible that the KO has more BK given that the width at 1/3 height of the first spike is narrower in the KO before paxilline. After paxilline application has removed the BK contribution to the spike train, the width is no longer significantly different for the first spike. The significant differences in the width of the second spike are also interesting but probably not related to BK. The widths are significantly different between WT and KO before paxilline application, but also after paxilline application when there should be no contribution from BK (Fig. 4.3B). This indicates that while BK differences may be affecting the initial spike, there is likely at least one other current that differentially affects the width of the second spike.

Chapter 5: Contribution of M channels in CA1 pyramidal neurons in FMR1 knockout mice

INTRODUCTION

In addition to Ca^{2+}-activated potassium channels, other potassium channels, such as the M channel, contribute to the after hyperpolarization, and therefore can effect spike frequency adaptation (Madison and Nicoll, 1984; Storm, 1989). Furthermore, mRNA for two of the subunits that form the M-channel, $K_V7.2$ and $K_V7.3$, are candidates for regulation by FMRP (Darnell et al., 2011). The M-channel activation range is controlled by several factors, including subunit composition, but tends to be slightly more depolarized than rest. For this reason most experiments were done holding the cell at -70 mV and again at -60 mV. Although at negative potentials, I_h can contribute to an after-hyperpolarization, initially no blocker was used because previous work (Brager et al., 2012) has shown no difference in I_h at the soma.

METHODS

Two sets of experiments were performed that differed in their internal solutions, ion channel blockers, and the concentration of M-channel blocker XE991. The first set of experiments used the standard internal and blockers as specified in the general methods section and 10 μM XE991 was used to block I_M. EPSPs were simulated using 2 exponential equations. Two additional protocols were used: 1) a 500 ms current injection adjusted to yield 8 spikes and 2) 5 1 ms current injections just large enough to invoke an action potential delivered at 100 Hz.

A second set of experiments were performed with an internal and blockers that were more similar to work done by (Shah et al., 2011) in an attempt to replicate her data

from rat in the mouse. For these experiments (in μM), K-gluconate was replaced with 120 KMeSO3, gabazine was replaced with 10 bicuculline and 1 CGP55845, and 3 XE991 was used instead of 10. In addition, 10 μM ZD7288 (ZD) was used to remove any AHP due to I_h. For these experiments, the EPSPs were simulated using an α function (Fig 5.1). The data from these experiments are shown with a gray background in the figures below.

The medium after-hyperpolarization (mAHP) was obtained by offsetting the trace so baseline is 0, and then finding the most negative value after the spike(s) once the trace has hyperpolarized below 0, within a 100 ms window after the end of the current injection. Analysis using the integral of this area below baseline yielded similar results (data not shown).

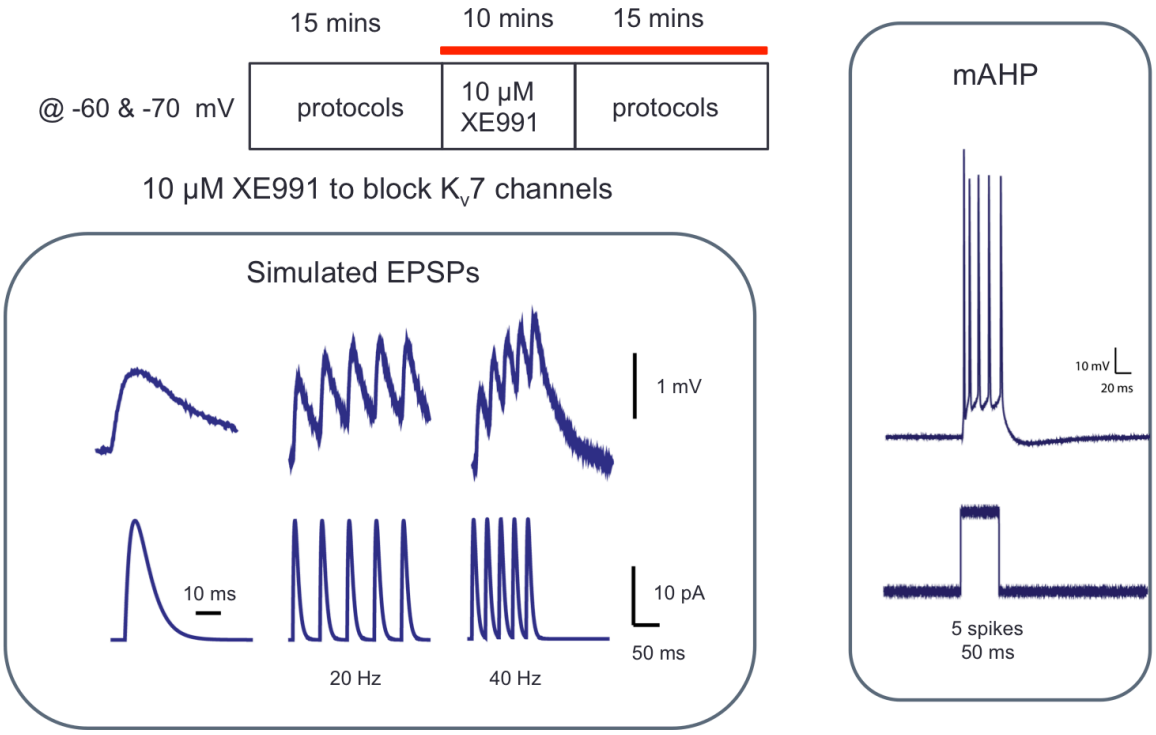

Figure 5.1: The timeline for the XE991 infusion and the protocols used for the simulated EPSPs and measuring the mAHPs.

EPSP summation was calculated as the amplitude of the fifth EPSP divided by the amplitude of the first EPSP.

Data was sampled at 50 kHz and filtered at 20 kHz.

Student's t-test with repeated measures was used to determine significant differences before and after drug application.

RESULTS

Resting membrane potential was significantly different before and after application of XE991 (Fig. 5.2A) for the WT (p=0.0014) and KO (p=0.03). In addition the steady state input resistance (Fig 5.2B) was significantly different before and after drug application for the WT at -70 mV (p=0.012) and for the KO at both -60 mV (p=0.016) and -70 mV (p=0.011).

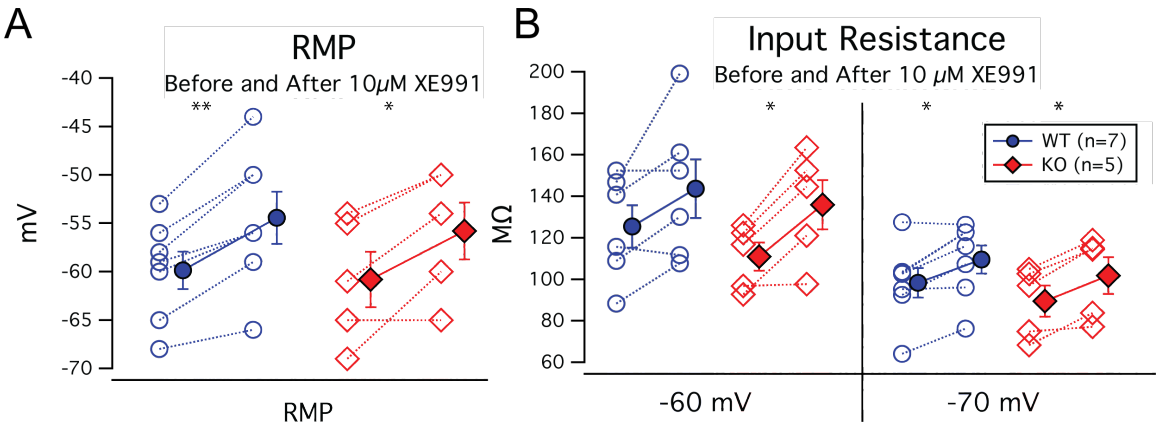

Figure 5.2: Resting membrane potential and input resistance for WT and KO before and after 10 μM XE991 (* p<0.05).

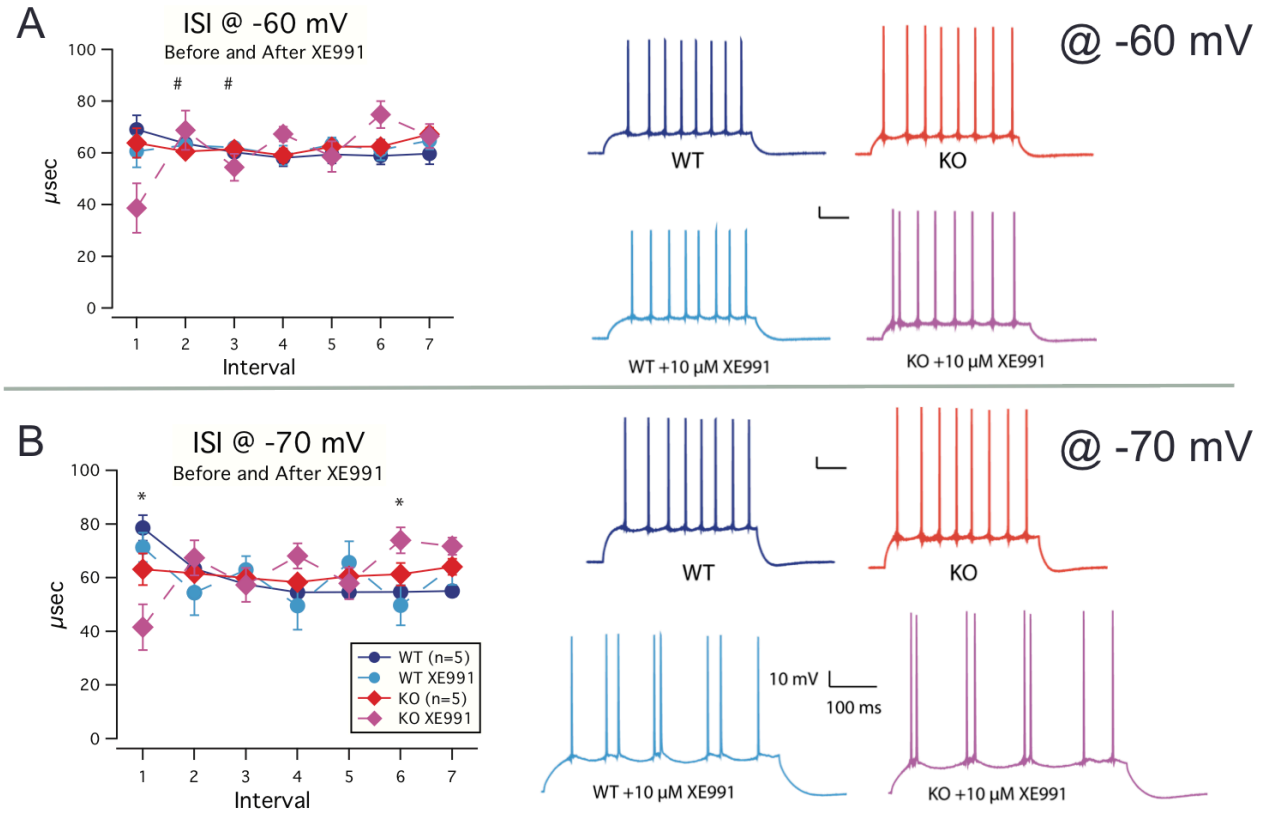

Figure 5.3: Interspike interval for 8 spikes in WT and KO before and after 10 μM XE991. A, ISI at -60 mV holding potential and sample traces (# indicates difference in variance of the measurments after XE991). B, ISI at -70 mV holding potential and sample traces (*: $p<0.05$ between KO after XE991 and both WT measurements).

A 500 ms current injection, adjusted to elicit 8 spikes, was used to measure inter-spike intervals (ISI). At a holding potential of -60 mV (Fig 5.3A), there were no significant differences between WT and KO before and after drug application. However, the data points for the second and third intervals after drug application had different variances. At -70 mV (Fig 5.3B), there were some significant differences. For the first interval, the KO after XE991 was significantly different from the WT both before ($p=0.0053$) and after XE991 ($p=0.019$). Similarly for the 6th interval, the KO after XE991

differed significantly from the WT both before (p=0.0054) and after XE991 (p=0.026). Although only significant for the -70 mV holding potential, at both holding potentials the ISI in the KO after drug was smaller than the WT. In both the WT and KO after drug, the cells had a propensity to fire in bursts of 2 spikes. Interestingly, the KO tended to fire two spikes initially while the WT fired one spike initially before transitioning to a 2 spike bursting mode.

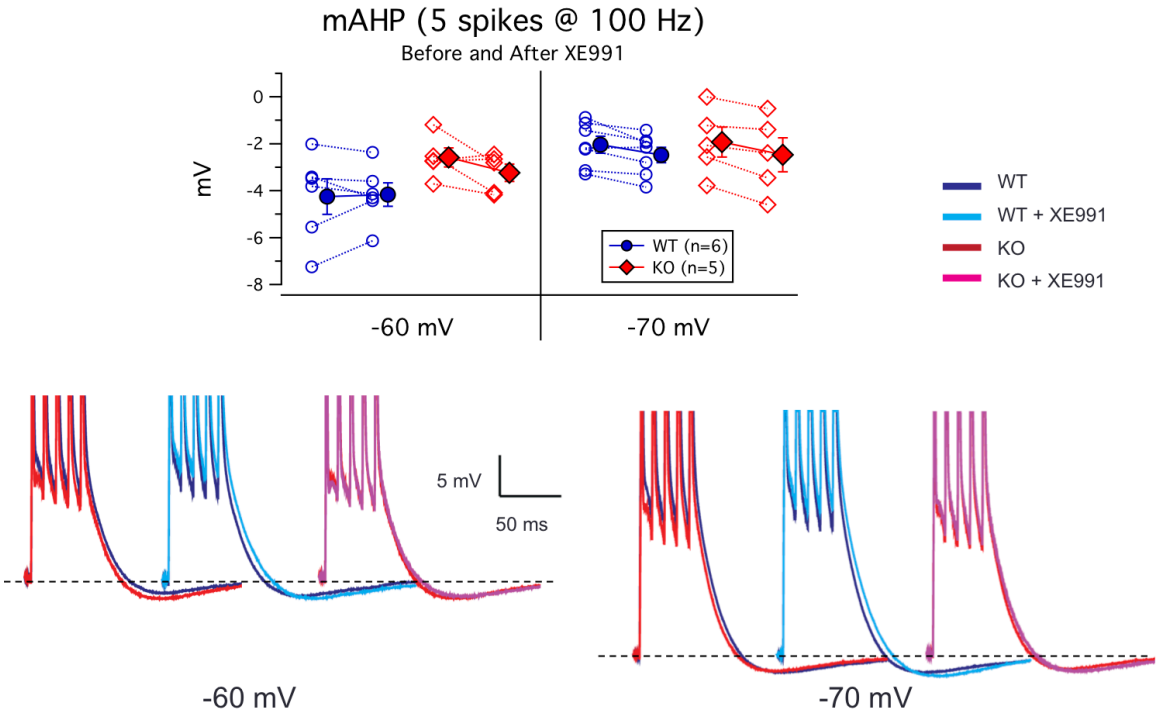

Figure 5.4: Medium AHP measurements from a burst of 5 spikes at 100 Hz for WT and KO before and after 10 μM XE991. There were no significant differences.

To evaluate the medium AHP (mAHP) directly, a protocol consisting of a burst of 5 spikes delivered at 100 Hz was used. This protocol was executed from holding potentials of both -60 and -70 mV. Although the data are not significantly different among the conditions (genotype or drug), the trend was for the mAHP to get larger (i.e.

more hyperpolarized) contrary to expectations (Fig. 5.4). To further evaluate the effectiveness of XE991, internal solutions, synaptic blockers and XE991 concentration were changed to be more similar to that in existing published work, and ZD7288 was used to remove any AHP due to I_h. This condition is referred to as "modified internal" in the text and with "+ZD" and on a gray background in graphs.

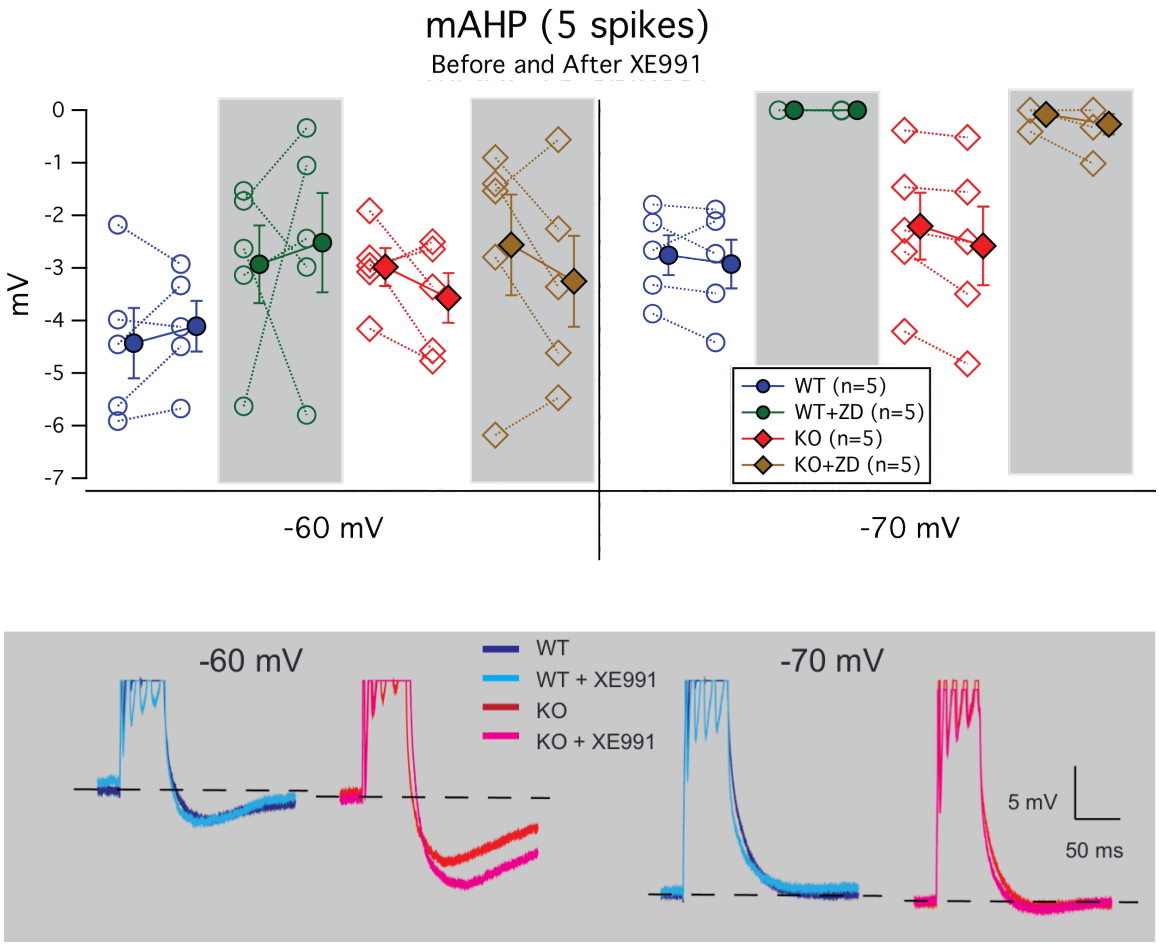

Figure 5.5: Medium AHP for both sets of conditions (normal and modified internal). Example traces shown.

Using the 50 ms protocol, where the current is adjusted to elicit 5 spikes, the mAHP was obtained as the offset from baseline. At -70 mV, the new conditions, which

included ZD, removed most occurrences of a medium AHP (Fig 5.5). At -60 mV, while no significant differences occurred, the trend of the averaged data for both conditions differed between WT and KO. The WT had a reduction in mAHP whereas the KO had an increase in mAHP.

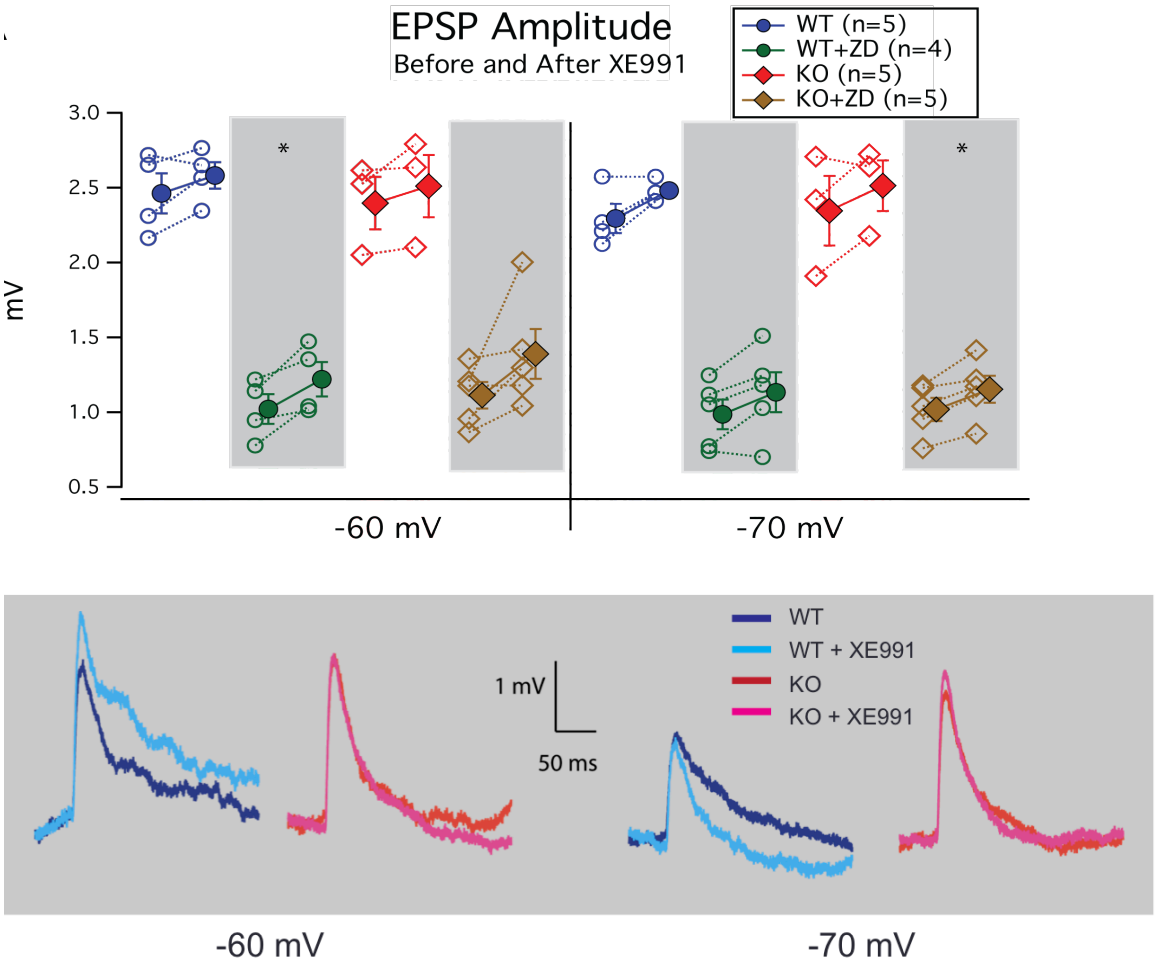

Figure 5.6: EPSP amplitude for both sets of conditions (normal and modified internal) with sample traces.

Simulated EPSPs were also used to evaluate the M current in the KO and WT. For single EPSPs, the trend for both WT and KO was an increase in amplitude after application of XE991 (Fig 5.6). Only two conditions showed significant differences in a

repeated measures t-test: the WT with normal internal at -60 mV (p=0.045) and the KO with modified internal at -70 mV (p=0.0107). For the summation protocols, there were no significant differences between WT and KO before or after drug application within either normal or modified internal (Fig 5.7, 5.8).

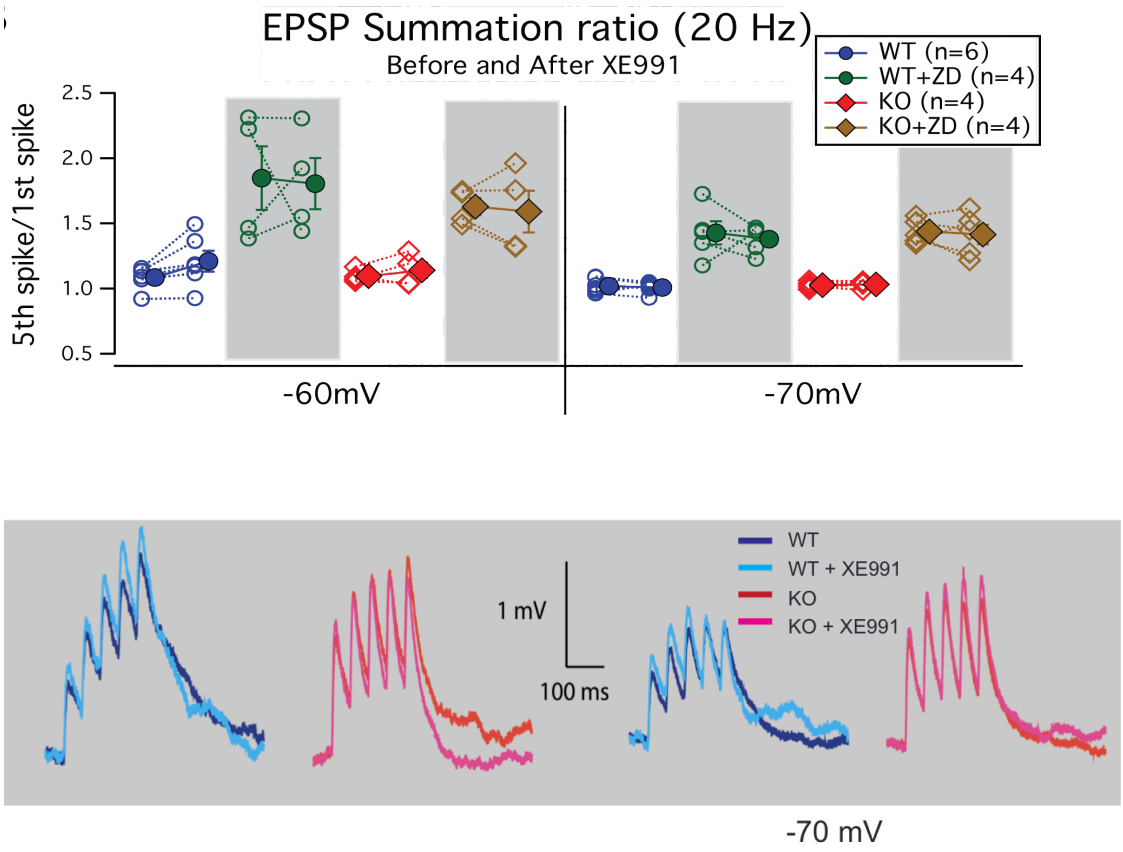

Figure 5.7: EPSP summation ratio at 20 Hz for both sets of conditions (normal and modified internal) with sample traces.

DISCUSSION

Applying the M-channel blocker, XE991, had a similar effect for WT and KO in that it led to a 2-spike burst. This is in agreement with previous work in the rat (Yue and Yaari, 2004). There was a difference in the bursting pattern however, where the KO

tended to start with a doublet, while the WT tended to start with a single spike before transitioning into doublets. It is not clear what causes the continuation of the doublets; however, they were common in both WT and KO after drug application.

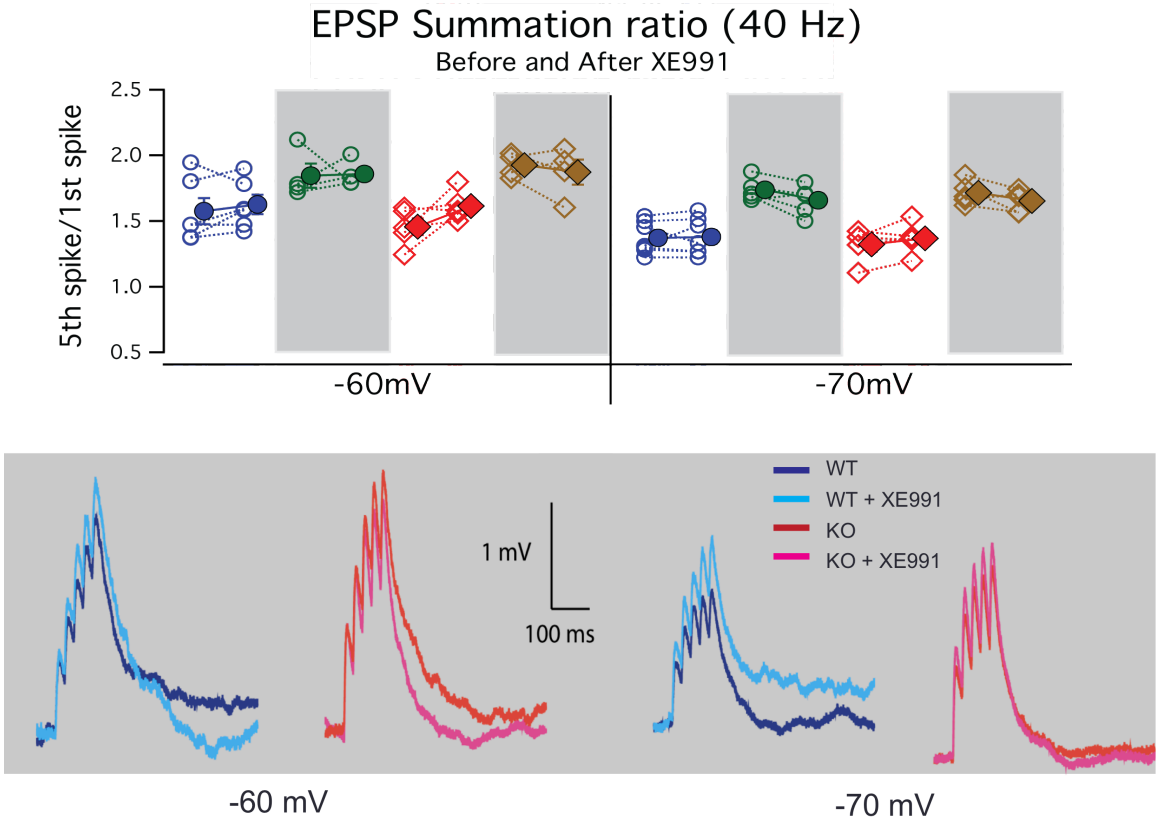

Figure 5.8: EPSP summation ratio at 40 Hz for both sets of conditions (normal and modified internal) with sample traces.

On the other hand, two protocols that typically yield differences in rat after application of XE991 did not result in differences in either WT or KO mice. A measure of mAHP resulted in differing trends between the WT and KO, but none of these differences were significant (Fig 5.5). Experiments looking at the height of a single simulated EPSP and the summation of 5 EPSPs were performed to analyze the changes in both the WT and KO before and after XE991 (Fig 5.6). Previous work in rat showed that

applying XE991 leads to a significant increase in summation of EPSPs delivered at 20 Hz and 40 Hz when the neuron is held at -60 mV (Shah et al., 2011). These experiments in mice show no significant differences in summation. In addition, only two of the eight EPSP amplitude measurements were significantly different before and after XE991. Differences in resting potential and input resistance in both WT and KO after XE991 application indicate that the drug did have an effect on the neurons (Fig 5.1). One possible explanation of why XE991 did not produce all the expected results is that M channels might not located peri-somatically in the mouse as they are in the rat. Therefore changes due to the drug in the mouse would not be seen as readily when measured at the soma. Another possibility is that the neither of the internal solutions used are effective at showing I_M effects. One recommendation would be to use $KMeSO_4$ instead of either the K-gluconate or $KMeSO_3$ that was used here. Thirdly, there might be a difference in M channel subunit composition between the rat and mouse that yields these differing results.

Chapter 7: Discussion

In general, the differences in the firing properties between a FMR1 KO mouse and a WT mouse are fairly subtle. They are most easily seen when looking at spike frequency adaptation and spike amplitude attenuation in a train of spikes.

The investigation of differential contributions of BK could be enhanced by a larger data set and by the addition of biochemistry measures for αBk, Bk β4 and Bk β2. In addition, experiments using iberiotoxin could be used to investigate differences in αBk or Bk β2.

The investigation of M current contributions yielded some confusing results based on the unexpeceted outcomes to some of the measurements after infusion of XE991. It would be worth investigating differences between a WT mouse and rat, and establishing a solid baseline of expected results in mice before continuing work with the FMR1 KO mouse. This investigation could also be enhanced with some biochemistry assays for Kv7.2 and Kv7.3.

When interpreting the inter-spike interval (ISI) data it is useful to consider possible effects of BK and M channels together. The BK data suggests that it is most influential after the first spike in a train. Experiments from the application of XE991, which cause the removal of M current, yield a bursting pattern that is most variable for the first ISI. The M current that is present in the BK experiments could be a compensatory mechanism that may be occluding spike timing differences due to BK. If the KO truly does have more BK than the WT, then the KO could have a doublet because of the quick repolarization and recovery of Na channels from inactivation. In the non-drug scenario presumably the M current is maintaining a more hyperpolarized membrane

potential, which spreads out the timing between the first 2 spikes. It would be interesting to see the effect of paxilline and XE991 together in the KO and WT mice.

Finally, the data indicating a decrease in the initial rate of rise in the KO are compelling. However, to date it has been very difficult to get consistent results among the techniques used to study I_{Na} at the axon initial segment. As techniques are improved and new methods become available, the impact on the AIS of the missing FMR1 protein should be explored.

References

Anon (1994) Fmr1 knockout mice: a model to study fragile X mental retardation. The Dutch-Belgian Fragile X Consortium. Cell 78:23–33.

Bean BP (2007) The action potential in mammalian central neurons. Nat Rev Neurosci 8:451–465.

Bear MF, Huber KM, Warren ST (2004) The mGluR theory of fragile X mental retardation. Trends Neurosci 27:370–377.

Bell MV, Hirst MC, Nakahori Y, MacKinnon RN, Roche A, Flint TJ, Jacobs PA, Tommerup N, Tranebjaerg L, Froster-Iskenius U (1991) Physical mapping across the fragile X: hypermethylation and clinical expression of the fragile X syndrome. Cell 64:861–866.

Brager DH, Akhavan AR, Johnston D (2012) Impaired Dendritic Expression and Plasticity of h-Channels in the fmr1−/y Mouse Model of Fragile X Syndrome. Cell Reports.

Brown MR, Kronengold J, Gazula V-R, Chen Y, Strumbos JG, Sigworth FJ, Navaratnam D, Kaczmarek LK (2010) Fragile X mental retardation protein controls gating of the sodium-activated potassium channel Slack. Nat Neurosci 13:819–821.

Darnell JC, Van Driesche SJ, Zhang C, Hung KYS, Mele A, Fraser CE, Stone EF, Chen C, Fak JJ, Chi SW, Licatalosi DD, Richter JD, Darnell RB (2011) FMRP Stalls Ribosomal Translocation on mRNAs Linked to Synaptic Function and Autism. Cell 146:247–261.

Galvez R, Greenough WT (2005) Sequence of abnormal dendritic spine development in primary somatosensory cortex of a mouse model of the fragile X mental retardation syndrome. Am J Med Genet A 135:155–160.

Gross C, Yao X, Pong DL, Jeromin A, Bassell GJ (2011) Fragile X mental retardation protein regulates protein expression and mRNA translation of the potassium channel Kv4.2. J Neurosci 31:5693–5698.

Grossman AW, Elisseou NM, McKinney BC, Greenough WT (2006) Hippocampal pyramidal cells in adult Fmr1 knockout mice exhibit an immature-appearing profile of dendritic spines. Brain Res 1084:158–164.

Gu N, Vervaeke K, Storm JF (2007) BK potassium channels facilitate high-frequency firing and cause early spike frequency adaptation in rat CA1 hippocampal pyramidal cells. J Physiol (Lond) 580:859–882.

Huber KM (2002) Altered synaptic plasticity in a mouse model of fragile X mental retardation. Proceedings of the National Academy of Sciences 99:7746–7750.

Lancaster B, Adams PR (1986) Calcium-dependent current generating the afterhyperpolarization of hippocampal neurons. J Neurophysiol 55:1268–1282.

Lancaster B, Nicoll RA (1987) Properties of two calcium-activated hyperpolarizations in rat hippocampal neurones. J Physiol (Lond) 389:187–203.

Lee HY, Ge W-P, Huang W, He Y, Wang GX, Rowson-Baldwin A, Smith SJ, Jan YN, Jan LY (2011) Bidirectional Regulation of Dendritic Voltage-Gated Potassium Channels by the Fragile X Mental Retardation Protein. Neuron 72:630–642.

Madison DV, Nicoll RA (1984) Control of the repetitive discharge of rat CA 1 pyramidal neurones in vitro. J Physiol (Lond) 354:319–331.

Poolos NP, Johnston D (1999) Calcium-activated potassium conductances contribute to action potential repolarization at the soma but not the dendrites of hippocampal CA1 pyramidal neurons. J Neurosci 19:5205–5212.

Shah MM, Migliore M, Brown DA (2011) Differential effects of Kv7 (M-) channels on synaptic integration in distinct subcellular compartments of rat hippocampal pyramidal neurons. J Physiol (Lond) 589:6029–6038.

Storm JF (1987) Action potential repolarization and a fast after-hyperpolarization in rat hippocampal pyramidal cells. J Physiol (Lond) 385:733–759.

Storm JF (1989) An after-hyperpolarization of medium duration in rat hippocampal pyramidal cells. J Physiol (Lond) 409:171–190.

Storm JF (1990) Potassium currents in hippocampal pyramidal cells. Prog Brain Res 83:161–187.

Strumbos JG, Brown MR, Kronengold J, Polley DB, Kaczmarek LK (2010) Fragile X mental retardation protein is required for rapid experience-dependent regulation of the potassium channel Kv3.1b. J Neurosci 30:10263–10271.

Yue C, Yaari Y (2004) KCNQ/M channels control spike afterdepolarization and burst generation in hippocampal neurons. J Neurosci 24:4614–4624.